Anatomy and Cell Biology Publications   Anatomy and Cell Biology Department

9-1-2022

Planning system for the optimization of electric field delivery using implanted electrodes for brain tumor control

Erin Iredale

Brynn Voigt

Adam Rankin

Kyungho W Kim

Jeff Z Chen

See next page for additional authors

Authors

Erin Iredale, Brynn Voigt, Adam Rankin, Kyungho W Kim, Jeff Z Chen, Susanne Schmid, Matthew O Hebb, Terry M Peters, and Eugene Wong

RESEARCH ARTICLE

Planning system for the optimization of electric field delivery using implanted electrodes for brain tumor control

Erin Iredale[1] | Brynn Voigt[2] | Adam Rankin[3] | Kyungho W. Kim[2] | Jeff Z. Chen[1] | Susanne Schmid[4] | Matthew O. Hebb[4,5] | Terry M. Peters[1,3] | Eugene Wong[1,2]

[1]Department of Medical Biophysics, Schulich School of Medicine and Dentistry, Western University, London, Ontario, Canada

[2]Department of Physics and Astronomy, Western University, London, Ontario, Canada

[3]Robarts Research Institute, Schulich School of Medicine and Dentistry, Western University, London, Ontario, Canada

[4]Department of Anatomy and Cell Biology, Schulich School of Medicine and Dentistry, Western University, London, Ontario, Canada

[5]Department of Clinical Neurological Sciences, Schulich School of Medicine and Dentistry, Western University, London, Ontario, Canada

Correspondence
Erin Iredale, Department of Medical Biophysics, Schulich School of Medicine and Dentistry, Western University, London, Ontario, Canada.
Email: eiredale@uwo.ca

Funding information
Natural Sciences and Engineering Research Council of Canada; Cancer Research Society; Canada Foundation for Innovation; Western Innovation Fund

Abstract

Background: The use of non-ionizing electric fields from low-intensity voltage sources (< 10 V) to control malignant tumor growth is showing increasing potential as a cancer treatment modality. A method of applying these low-intensity electric fields using multiple implanted electrodes within or adjacent to tumor volumes has been termed as intratumoral modulation therapy (IMT).

Purpose: This study explores advancements in the previously established IMT optimization algorithm, and the development of a custom treatment planning system for patient-specific IMT. The practicality of the treatment planning system is demonstrated by implementing the full optimization pipeline on a brain phantom with robotic electrode implantation, postoperative imaging, and treatment stimulation.

Methods: The integrated planning pipeline in 3D Slicer begins with importing and segmenting patient magnetic resonance images (MRI) or computed tomography (CT) images. The segmentation process is manual, followed by a semi-automatic smoothing step that allows the segmented brain and tumor mesh volumes to be smoothed and simplified by applying selected filters. Electrode trajectories are planned manually on the patient MRI or CT by selecting insertion and tip coordinates for a chosen number of electrodes. The electrode tip positions and stimulation parameters (phase shift and voltage) can then be optimized with the custom semi-automatic IMT optimization algorithm where users can select the prescription electric field, voltage amplitude limit, tissue electrical properties, nearby organs at risk, optimization parameters (electrode tip location, individual contact phase shift and voltage), desired field coverage percent, and field conformity optimization. Tables of optimization results are displayed, and the resulting electric field is visualized as a field-map superimposed on the MR or CT image, with 3D renderings of the brain, tumor, and electrodes. Optimized electrode coordinates are transferred to robotic electrode implantation software to enable planning and subsequent implantation of the electrodes at the desired trajectories.

Results: An IMT treatment planning system was developed that incorporates patient-specific MRI or CT, segmentation, volume smoothing, electrode trajectory planning, electrode tip location and stimulation parameter optimization, and results visualization. All previous manual pipeline steps operating on diverse software platforms were coalesced into a single semi-automated 3D Slicer-based user interface. Brain phantom validation of the full system implementation was successful in preoperative planning, robotic electrode implantation, and postoperative treatment planning to adjust stimulation parameters based on

actual implant locations. Voltage measurements were obtained in the brain phantom to determine the electrical parameters of the phantom and validate the simulated electric field distribution.

Conclusions: A custom treatment planning and implantation system for IMT has been developed in this study and validated on a phantom brain model, providing an essential step in advancing IMT technology toward future clinical safety and efficacy investigations.

KEYWORDS
brain tumor, electric field, electrotherapy, glioblastoma, optimization, treatment planning system

1 | INTRODUCTION

Electric fields from low-intensity voltage sources are showing increasing promise as a treatment modality for brain cancer.[1–10] Intratumoral modulation therapy (IMT) is an emerging technique intended to restrict tumor growth by applying low-intensity electric fields using bioelectrodes implanted within or adjacent to tumor volumes.[7–10] Preclinical in vitro and in vivo investigations into the application of 200 kHz, low-intensity ($\pm$ 2.00 V stimulation) electric fields to glioblastoma (GBM) and diffuse intrinsic pontine glioma (DIPG) cells have shown the efficacy of this modality as a monotherapy,[9] and in conjunction with chemotherapy and radiation.[8] A single stimulating electrode paradigm was implemented in these early studies but computer simulations and optimization studies have since prompted the use of multiple stimulating electrodes with optimized relative phase shifts of input waveforms to increase the coverage capacity of the IMT fields.[7] The previous IMT optimization study[7] established a method for temporally maximizing tumor coverage from IMT electric fields. This algorithm allowed for electrode location and stimulation phase shift parameters to be optimized for multiple electrodes, each with multiple separately programmable contacts. The phase shifting of each electrode contacts' sinusoidal voltage waveform creates an electric field that rotates in 3D in both directionality and intensity, over the waveform period. A simplified spherical tumor model with parallel electrodes was used in this previous study, which requires extension into patient-specific models with non-parallel electrodes defined by insertion and tip coordinates.

While the primary mechanism of low-intensity electric fields has yet to be definitively elucidated, there are a number of mechanisms that have been suggested to play a role in selective tumor control. These include antimitotic mechanisms, enhanced cell membrane permeability, increased immunogenic cell death, impairment of DNA repair, antimigratory, and autophagic influences.[11–15] The most well-supported theories remain antimitotic, where mitotic spindle and septin ring formation are impacted in metaphase and cytokinesis respectively,[16–18] and impact on cell membrane permeability, which has been observed experimentally.[19] While the synergistic mechanisms of action and their effects on tumor control are still under investigation, the applied electric field is the basis of each proposed mechanism. With tumor control found experimentally to depend on electric field intensity and frequency,[17] maximizing the tumor coverage with threshold electric field magnitudes is the current therapy objective.

A review of the published literature on treatment planning systems that simulate the electric field from electrode sources highlighted both external and internal electrode applications. The clinical use of an external electric field device for glioblastoma (NovoTTF™), using a treatment planning system (NovoTAL™)[2,4,20–22] establishes personalized array layouts, found through simulation studies to enhance electric field coverage to certain brain regions.[23] A recent optimization study of electric fields from the external device highlighted the importance of minimizing the anisotropy of electric field components while maintaining field intensity,[24] supporting the use of rotating fields in IMT. Similarly, both deep brain stimulation (DBS) to treat neurological disorders[25–30] and irreversible electroporation (IRE) to ablate tumor volumes[31–35] require electric field and implanted electrode trajectory planning to reach the target volume. Stereoelectroencephalography (SEEG) uses multiple depth electrodes implanted in the brain to identify seizure zones, with robotic and computer assisted trajectory planning gaining interest.[36–38] Treatment planning systems play a large role in radiotherapy, including brachytherapy,[39–46] where the radiation dose to patient-specific targets and organs at risk (OAR) are analyzed and treatments are planned accordingly. IMT differs from external electric fields devices in that electrodes are implanted directly in or adjacent tumor volumes, requiring trajectory planning of multiple electrodes. Advantages of long-term implanted IMT electrodes compared to external electric field devices are the potential for improved quality of life, similar to DBS which is well tolerated, and the potential to reach tumors deep in the brain. The goal of IMT is to cover a large tumor volume (>1 cm^3) with intermediate frequency (200 kHz) electric field using multiple electrodes,

to avoid neural activation, as opposed to DBS where a small volume (~ 1 mm^3) is commonly targeted by one or two low-frequency electrodes (~ 130 Hz) to initiate neural activation.[30] While the goal of electroporation is to ablate a tumor volume using multiple electrodes,[33] the permanent implantation and low-intensity nature of IMT fields requires additional optimization considerations, where we maximize the electric field tumor coverage with minimal input voltage, achieved by optimizing relative phase shifts of the delivered waveforms between electrode contacts.[7] Lastly, radiotherapy treatments consider the delivered ionizing radiation dose to the tumor volume and nearby organs at risk, whereas IMT considers nonionizing electric fields that interfere with one another. The differences between IMT and other modalities necessitate the creation of a custom treatment planning system for IMT.

To accompany ongoing in vitro and in vivo validations of IMT, the preparation for future single center patient safety and efficacy trials will require a way to plan animal and patient-specific electrode trajectories and stimulation programming to cover their tumor with a threshold electric field. Precursory pathways from preclinical to clinical investigations substantiate the need for a treatment planning system to be developed. To advance this technology to allow clinical testing, optimal treatment parameters and electrode configurations on a patient-specific basis are required. In this study, the treatment stimulation parameters and electrode placement is determined by designing a treatment planning system that utilizes and expands upon the IMT optimization algorithm previously established.[7] The goal of this study is to amalgamate the numerous steps in the optimization pipeline into a cohesive, user-friendly system using the 3D Slicer[47,48] platform and to validate the trajectories and plan in a brain phantom. All planning steps are accessed in a single application with ordered steps, with options for preoperative or postoperative planning, human or preclinical in vivo animal planning, and different electrode models (multi-contact cylindrical electrodes, custom electrode arrays, or preclinical multi-electrode wire constructs).

The completed system allows the user to upload, segment and smooth the patient magnetic resonance imaging (MRI) or computed tomography (CT) data, plan the electrode trajectories, and optimize the electrode tip location, phase shift, and voltage parameters. The treatment planning system was validated by completing a treatment plan on a phantom brain model and implanting the electrodes using a neurosurgical robot (Neuromate®)[49] to demonstrate the full treatment pipeline, encompassing implantation, field delivery, and postoperative planning adjustment. The IMT treatment planning system development provides an essential step in advancing future clinical studies.
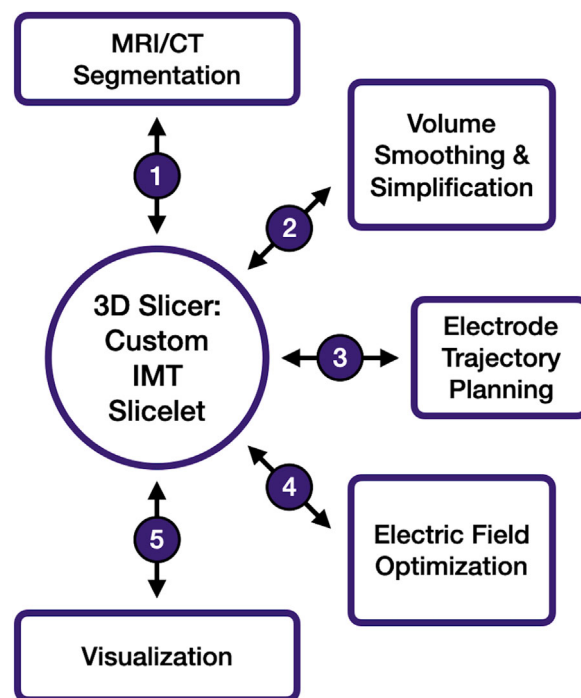

FIGURE 1 Pipeline of custom IMT Slicelet in 3D Slicer including the tissue segmentation, smoothing and simplification of segmented volumes (custom module), electrode trajectory planning (custom module), electric field optimization (custom module) and the visualization of the completed optimized treatment plan (custom module)

2 | MATERIALS AND METHODS

2.1 | Slicelet design

The user interface for the IMT treatment planning system was developed in a custom 3D Slicer application, called a Slicelet.[50] A Slicelet is a custom coded application that combines all necessary modules into a numbered pipeline. The design of the custom IMT Slicelet (Figure 1) begins with the setup, which includes patient selection and DICOM import (create new patient or open existing patient), the selection of patient type (human or preclinical), and the patient status (preoperative or postoperative) (Figure S1a).

After setup of the patient model, the planning process includes five main steps: (1) segmentation of brain, tumor, organ at risk, and surgical resection cavity volumes, (2) the smoothing of the segmented volumes, (3) the planning of electrode implantation coordinates, (4) the optimization of tip coordinates, phase shift and voltage amplitude, and (5) visualization of results. Step 1 is included as the built-in segmentation module in 3D slicer, where users can segment the brain and tumor regions using any of the existing 3D Slicer segmentation features including paint, draw, erase, level tracing, fill between slices, threshold, margin, smoothing and islands. Steps 2–4 are custom coded modules explained

in sections 2.2 and 2.3. Step 5 is the custom coded visualization module, which displays the numerical results of the optimization (electrode coordinates, phase shift, voltage amplitude) in tables. The electrode locations are also visualized as an interactive 3D model of the brain, tumor, and electrodes. An electric field volume histogram (EVH) is displayed showing the percent of tumor (and organ at risk) volume covered by at least the corresponding electric field. The resulting time average electric field maps are displayed on the MR or CT image as coronal, sagittal and axial interactive slices. Built-in 3D Slicer Models[51] and Volumes[52] modules were added to allow users to adjust the DICOM image parameters and 3D volume displays.

2.2 | Smoothing and electrode implantation modules

The custom smoothing module (Figure S1b) utilizes the Python command line interface to access selected MeshLab (v2021.05) filters to smooth and simplify brain, tumor, organ at risk, and surgical resection cavity volumes. The selected filter options include Quadratic Edge Collapse Decimation (simplification), Laplacian Smooth, HC Laplacian Smooth, Uniform Mesh Resampling, Clustering Decimation (simplification), Smooth Face Normals and Merge Close Vertices. A Run Filters button allows users to continue smoothing and simplifying with different filters until the target file size is reached (<100 kB). Real time display of the smoothed volumes and contours on image slice views are included to ensure accuracy is maintained and volumes have not been oversimplified.

The custom electrode implantation module (Figure S1c) uses the Python command line interface for the placement of fiducial points. Based on the number of electrodes selected, the locations of the insertion and tip coordinates for each electrode are selected on the MR or CT image by the user. Also included is the ability to import existing electrodes.

2.3 | Optimization module

The optimization module (Figure S1d) requires connection to preexisting MATLAB (v2021a) code[7] that communicates with COMSOL Multiphysics (v5.4) for model creation and electric field computation at each iteration using the COMSOL-MATLAB Livelink. A MATLAB function was created to connect to the Livelink automatically and run the optimization code. This function is connected to the 3D Slicer module graphical user interface (GUI) inputs using the 3D Slicer MATLAB Bridge. The existing optimization code was updated to automatically generate a unique COMSOL model based on the user inputs at the start of an optimization

(smoothed volumes, patient type (human or preclinical), preoperative or postoperative, organ at risk or resection cavity presence). The COMSOL model build generates cylindrical multi-contact electrodes with customizable contact height, spacing, and radius, with default values included (0.800 mm radius, 5.00 mm contact height, 1.00 mm contact spacing) for human models, or wire electrodes (0.125 mm radius, 3.00 mm contact height) for preclinical models.

To automatically generate cylindrical electrodes in COMSOL, the insertion coordinate, electrode length, and spherical coordinates of the electrode trajectory are required. Electrode length (Equation 1), and spherical coordinates Θ (Equation 2) and Φ (Equation 3) are calculated for each electrode using the insertion coordinates (x_{in}, y_{in}, z_{in}) and tip coordinates $(x_{tip}, y_{tip}, z_{tip})$.

$$L = \sqrt{(x_{in} - x_{tip})^2 + (y_{in} - y_{tip})^2 + (z_{in} - z_{tip})^2}, \quad (1)$$

$$\Theta = \cos^{-1}\left[-\frac{(z_{in} - z_{tip})}{L}\right], \quad (2)$$

$$\Phi = -\frac{y_{in} - y_{tip}}{|y_{in} - y_{tip}|}\cos^{-1}\left[-\frac{x_{in} - x_{tip}}{\sqrt{(x_{in} - x_{tip})^2 + (y_{in} - y_{tip})^2}}\right]. \quad (3)$$

Contacts are generated along the electrode length by using calculated coordinates (x_c, y_c, z_c) for each contact based on the contact spacing cs, contact length cl and contact number n (Equation 4).

$$x_c = x_{in} + (x_{tip} - x_{in})\left[\frac{L - n(cl + cs) - cs}{L}\right]. \quad (4)$$

At each iteration of the pattern search optimization, the electric field is calculated from the COMSOL model for the list of iteration parameters. The mesh size for all geometrical entities is dependent on the material, with electrodes and contacts as a fine mesh size (1.73–13.8 mm element size), tumor as a normal mesh (3.11–17.3 mm element size), and surrounding brain as a course mesh (4.84–25.9 mm element size). Validation of the material dependent mesh sizes was completed to ensure convergence to the more accurate solution using the finest material independent mesh sizes (0.035–3.5 mm). The use of different mesh sizes allows for preservation of accuracy within the tumor volume and around electrodes while minimizing nodes in the surrounding brain to improve computation time. The electric field is computed using COMSOL's AC/DC

electric currents module, in the frequency domain at 200 kHz. To improve computation time, the electric field "kernel" is computed for each electrode contact at 1 V with all remaining contacts at 0 V. This allows for the superposition of electric field (summation of electric field vectors from each voltage source contribution) to be used to compute the electric field distribution in MATLAB for the set of phase shift and voltage amplitude parameters for that geometry. For each electrode location change, the "kernel" fields are calculated in COMSOL, and for each phase shift or voltage change, only the superposition calculation is required as the "kernel" fields only need to be calculated upon a location change.

The previous requirement for manual MATLAB command line inputs was removed and replaced by buttons and boxes in the Slicelet GUI. The necessary inputs are set to default values, and include voltage amplitude limit (2 V), prescription electric field (1 V/cm), brain and tumor electrical conductivity and dielectric (0.25 S/m and 3000 for brain, 0.24 S/m and 2000 for tumor[23,53–60]), nearby organ at risk, the electrical properties and weighting factor of the organ at risk, and electrical properties of a surgical resection cavity. The choice of optimization type includes two options per electrode optimization: phase shift only or location + phase shift. Three options are included for individual contact optimization: phase shift only, voltage amplitude only, or phase shift + voltage amplitude. The desired field coverage percentage, the use of a random starting point, and the option to save the COMSOL model file are all additional user selections.

Initial geometrical conditions for the optimization of electrode trajectories and programming are the user selected insertion and tip coordinates of each electrode. Insertion coordinates remain fixed, and the tip coordinates are an optimization variable, along with phase shift and voltage amplitude. A gradient free pattern search technique was used in the planning system, due to the nonconvexity of the objective function,[7] to broadly search parameter space. The success of an iteration at finding an improved objective value determines if parameter step size is increased (successful) or decreased (unsuccessful) at the next iteration. The pattern search algorithm first minimizes the objective function f (Equation 5), which maximizes the voxels covered by the prescription electric field E_{pres} while simultaneously maximizing the electric field of uncovered voxels and minimizing the electric field to nearby organs at risk.

$$f = \frac{1}{N_s} \sum_{j \varepsilon s} H\left(E_{pres} - \bar{E}_j\right)\left(\bar{E}_j - E_{pres}\right)^2 + w\frac{1}{N_{OAR}} \sum_{i \varepsilon OAR} \bar{E}_i^2.$$

$$(5)$$

The Heaviside function (H) term differentiates tumor voxels j covered and uncovered by the prescription field, and the squared difference term weighs voxels with time average electric field $\bar{E}_j$ closer to the prescription field preferably. The weighted OAR term minimizes the time

average field $\bar{E}_i$ to the OAR voxel i. The OAR weighting factor w is by default 0 unless an OAR is present. N_s represents the number of voxels in the tumor, and N_{OAR} is the number of voxels in the organ at risk volume.

The optimization of electric field conformity is included as a second step, to minimize the power consumption of active electrode contacts and to shape the field in 3D, by minimizing the electric field outside of the tumor while maintaining field coverage inside the tumor. The default objective function f (Equation 5) is changed to the inverse conformity index CI^{-1} (Equation 6) when this option is selected:

$$C I^{-1} = \frac{V_{E_{pres}}}{TV_{E_{pres}}},$$

$$(6)$$

where $V_{E_{pres}}$ is the total volume covered by at least the prescription electric field, and $VT_{E_{pres}}$ is the tumor volume covered by at least the prescription electric field. The inverse of the conformity index objective CI^{-1} is minimized by the pattern search algorithm, to minimize the electric field outside of the tumor. Display boxes show the prescription field coverage percentage and conformity index of the optimized electric field.

2.4 | Planning system testing

The complete treatment planning system pipeline was tested using two DICOM MRI data sets: a sample built-in 3D Slicer T1-weighted MRI of a human brain with a 3.5 cm diameter tumor,[61] and a T1-weighted MRI of a realistic brain phantom with a 1.9 cm diameter tumor in the frontal lobe (Synaptive Simulate, Toronto Canada).[62] The human MRI was used to test the human preoperative, postoperative surgical resection cavity, and preoperative with organ at risk planning pathways. The phantom MRI was used to test the human preoperative pathway using single and multiple insertion sites. The brain and tumor visible on MR images manually segmented using the paint, fill between slices, draw, and smoothing features. The electrode dimensions used for the phantom model were customized in the planning system to mimic AdTech SEEG electrodes (Surgi-One Medical Technologies Inc.; 0.430 mm radius, 2.29 mm contact height, 1.71 mm spacing). SEEG electrodes (0.860 mm diameter) were chosen over larger diameter DBS electrodes (1.27 mm)[63] based on the contact height and number of contacts per electrode (10) that would be sufficient to cover tumors with IMT fields. Optimization parameters for these models were chosen as the default values with a voltage limit of 4.00 V, prescription electric field of 1 V/cm, 95.0% desired tumor coverage, brain conductivity 0.25 S/m, brain dielectric 3000, tumor conductivity 0.24 S/m, and tumor dielectric 2000.[23,53–60]

2.5 | Phantom electrode implantation

Validation of the full pipeline implementation included a preoperative CT of a brain phantom (Synaptive), used to plan the tip coordinates, phase shift and voltage amplitude of a four-electrode, dual entry model on a virtual 1.7 cm diameter tumor. The insertion and optimized tip coordinates, and planning CT were inputted into the neurosurgical robot's (Neuromate®) planning system (Neuroinspire™)[64] for registration to the robot coordinate system using the Neurolocate™ fiducial apparatus and frameless patient registration module. A 2.11 mm diameter cannula fixed to the robot arm with an adaptor was used to place each electrode. The phantom was secured to the robot table using a cranial stabilization frame (Mayfield®). Postimplantation CT imaging was performed on the phantom and analyzed for geometrical accuracy and postoperative treatment planning.

Electric field is established by applying voltages and their phase shifts across electrodes. For each electrode, phase shift and voltage programming were applied as per phase shift optimization and voltage scaling results for the phantom CT model, to deliver the 1 V/cm electric field treatment to the tumor. The voltage drop and simulated electric field distribution were validated by measuring the voltage at two measurement electrodes and various contacts on the stimulating electrodes. A four-channel waveform generator (Highland Technology T340 4-channel compact function generator) was programmed based on optimized voltage and phase shift parameters and connected to five contacts per stimulating electrode using custom BNC to five measurement probe cables. The voltage waveform at the measurement electrode locations was measured using a four-channel oscilloscope (Siglent SDS1104X-E). Uncertainties in voltage measurement values from the waveform generator and oscilloscope were added in quadrature as ±40 Hz for frequency and ±0.03 V for recording electrodes and ±0.05 V for measurement contacts on the active electrodes. Uncertainties in the computer simulations comprised uncertainty in electrical properties (phantom conductivity ±1.0 e-7 S/m, phantom dielectric ±1.0, electrode insulation ±1.0 e-4 S/m) and trajectory (±1.10 mm). A parameter sweep for all uncertainty parameters and the effects on voltage and electric field tumor coverage was performed for each measurement scenario to obtain electrode contact-specific simulation uncertainties.

3 | RESULTS

3.1 | Slicelet design

The completed custom IMT Slicelet (Figure S1) contains all necessary planning steps within the workflow illustrated by Figure 1. All components and modules of the custom IMT Slicelet were tested for functionality. No user interaction with external software was required and the entire user experience of IMT treatment planning was contained within the Slicelet. Live connection between 3D Slicer and the MATLAB-COMSOL Livelink during optimization was successfully observed.

3.2 | Smoothing and electrode implantation modules

The smoothing module was demonstrated on segmented volumes from the human and phantom MRI data sets. Brain and tumor volumes were smoothed and simplified to <100 kB and were successfully implemented in the patient-specific COMSOL model build. A combination of the filters included in the module was required to reduce the file size while maintaining accuracy of the segmentations. The electrode implantation module was also tested on the human and phantom MRI data sets. For the human case, six electrodes were placed on the MRI from two burr holes (three electrodes per entry point) by selecting the insertion and tip coordinates of each electrode. For the phantom scenario, four electrodes were placed from either a single insertion site or two different insertion sites.

3.3 | Optimization module

The five main optimization types (electrode phase shift, electrode location + phase shift, individual contact phase shift, individual contact voltage amplitude, and individual contact phase shift + voltage amplitude) were tested for functionality on the human and phantom models. Optimal parameters that provide the necessary tumor coverage by the prescribed electric field were determined by the optimization algorithm. Any electrode contacts that did not contribute to the tumor coverage were automatically turned off to minimize the number of active contacts. The different electrode models (human multi-contact cylindrical electrodes, human custom electrode array and preclinical electrode constructs) were operational within the COMSOL model build and MATLAB optimization algorithm. The scale voltage option increased the voltage applied to each electrode until the desired tumor coverage was achieved. The location change option successfully updated the electric field map display considering the change in electrode coordinates.

3.4 | Planning system testing

The full planning pipeline was tested on both human and phantom models. Upon completion of an optimization, the resulting stimulation parameter tables, electrode
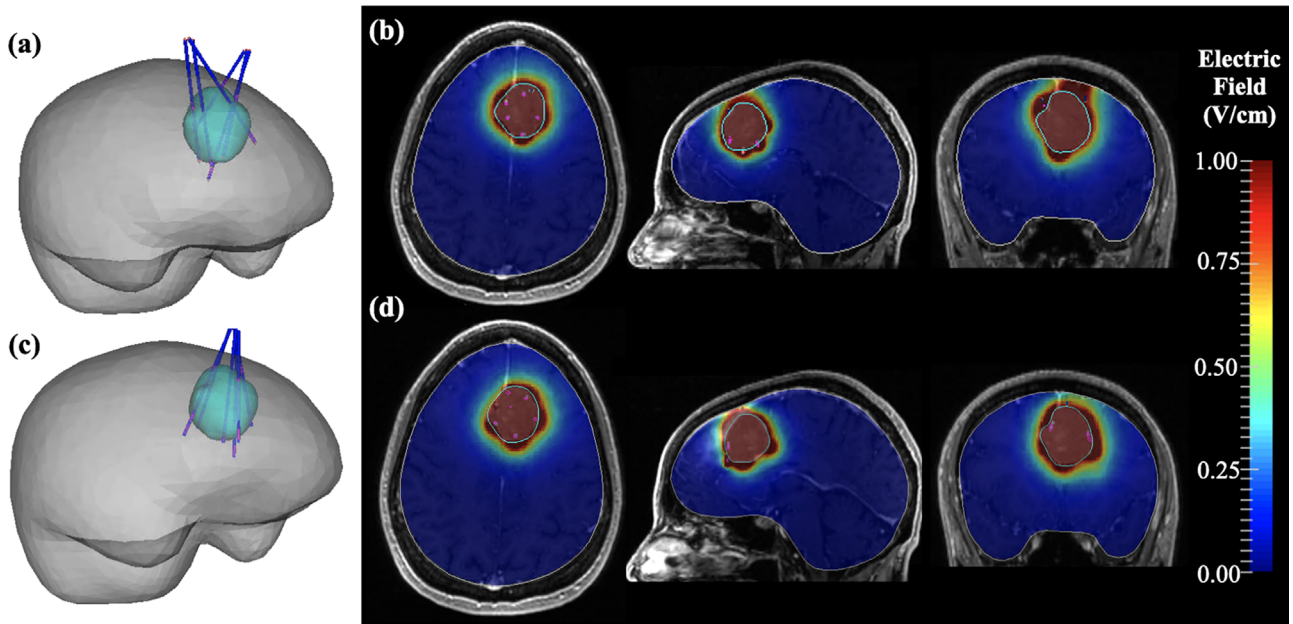
FIGURE 2 Results of electric field optimization for the (a) dual entry six-electrode human model with electrode location results displayed as the 3D geometry of brain (gray), tumor (cyan), electrodes (blue) and active contacts (magenta). The resulting electric fields (b) are displayed on selected axial, sagittal, and coronal cross sections superimposed on the MRI. Further numerical results of optimal phase shift, voltage amplitude, and electrode trajectories can be found in the supplementary materials (Figure S2). Results of electric field optimization for the (c) six-electrode single entry human model with 3D geometry and (d) resulting electric fields displayed on selected axial, sagittal and coronal cross sections superimposed on the MRI. Further numerical results of optimal phase shift, voltage amplitude, and electrode trajectories can be found in the supplementary materials (Figure S3)

coordinates table, electric field maps, 3D geometry, and EVH were displayed (Figures S2–S4). The results of a patient plan were accessible for future viewing by loading the visualization from the patient file. Full pipeline implementation using our planning system was achievable for the tested preoperative dual-entry human (Figure 2a and b), single-entry human (Figure 2c and d) and phantom models. The optimized results of the human dual-entry six electrode plan were electrodes spaced throughout the tumor volume (Figure 2a), covering 95.9% of the tumor volume with 1 V/cm, with a conformity index of 0.69. One electrode only required one active contact, one required three active contacts, one required four active contacts, and three required five active contacts. The voltage amplitude applied to active contacts ranged from 1.48 to 4.00 V, resulting in electric fields that were conformal to the tumor volume (Figure 2b). The optimized six electrode single entry human model contained electrodes evenly distributed through the tumor (Figure 2c), covering 95.6% of the tumor with 1 V/cm, with a conformity index of 0.69. Four electrodes required four active contacts, one required five, and one required six, with applied voltage amplitudes ranged from 0.63 V to 4.00 V, to shape the electric field to cover the tumor (Figure 2d).

All plans were set to cover 95.0% of the tumor volume with 1 V/cm, which was achieved in all cases. Conformity index optimization preserved this tumor coverage while decreasing the electric field outside of the tumor and

minimizing the number of active contacts. To optimize all parameters (electrode tip coordinates, individual contact phase shift, and voltage amplitude), the most efficient approach was to begin with the electrode location + phase shift optimization, followed by voltage scaling. The plan is further refined to determine optimal phase shift of the individual contacts on each electrode, and conformity index optimization of phase shift and voltage per electrode contact. Optimization results for all tested plans determined that electric fields could be shaped in 3D to cover the tumor volume over time.

3.5 | Phantom electrode implantation

Preoperative CT imaging was performed on the brain phantom and imported into the IMT treatment planning system, where a 1.7 cm diameter tumor was simulated. The optimization of electrode locations and phase shift of 2.20 V waveforms resulted in relative phase shifts of each electrode as 0°, 71.9°, 170.6°, and 235.3° to cover 96.1% of the tumor volume with 1 V/cm (Figure 3).

The phantom brain and skull were attached to the robot (Figure 4a) with the stabilization frame and the fiducial apparatus attached to the robot arm (Figure 4b). The phantom preoperative planning CT and planned electrode coordinates were registered to the robot operative setup CT with the planning system and frameless patient registration module. The four electrodes were
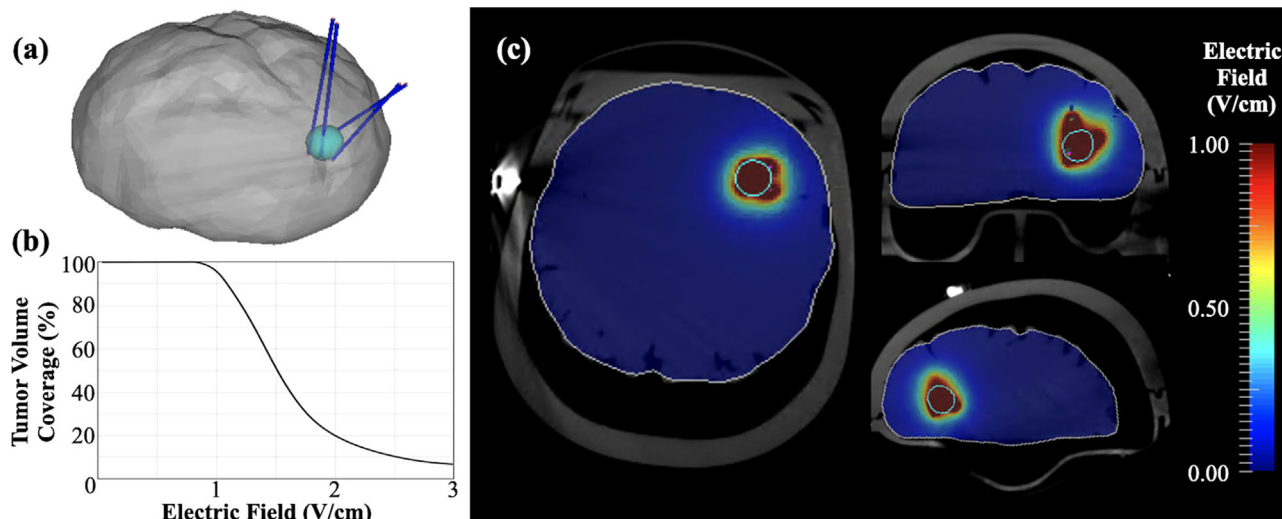
FIGURE 3 Results of electric field optimization for the four-electrode dual entry CT phantom model. Electrode location results displayed as (a) 3D geometry of brain (gray), tumor (cyan), electrodes (blue), and active contacts (magenta). Numerical electric field coverage results are displayed as the (b) EVH of tumor coverage, and (c) resulting electric fields are displayed on selected axial, coronal and sagittal cross sections superimposed on the phantom MRI. Further numerical results of optimal phase shift, voltage amplitude, and electrode trajectories can be found in the supplementary materials (Figure S4)
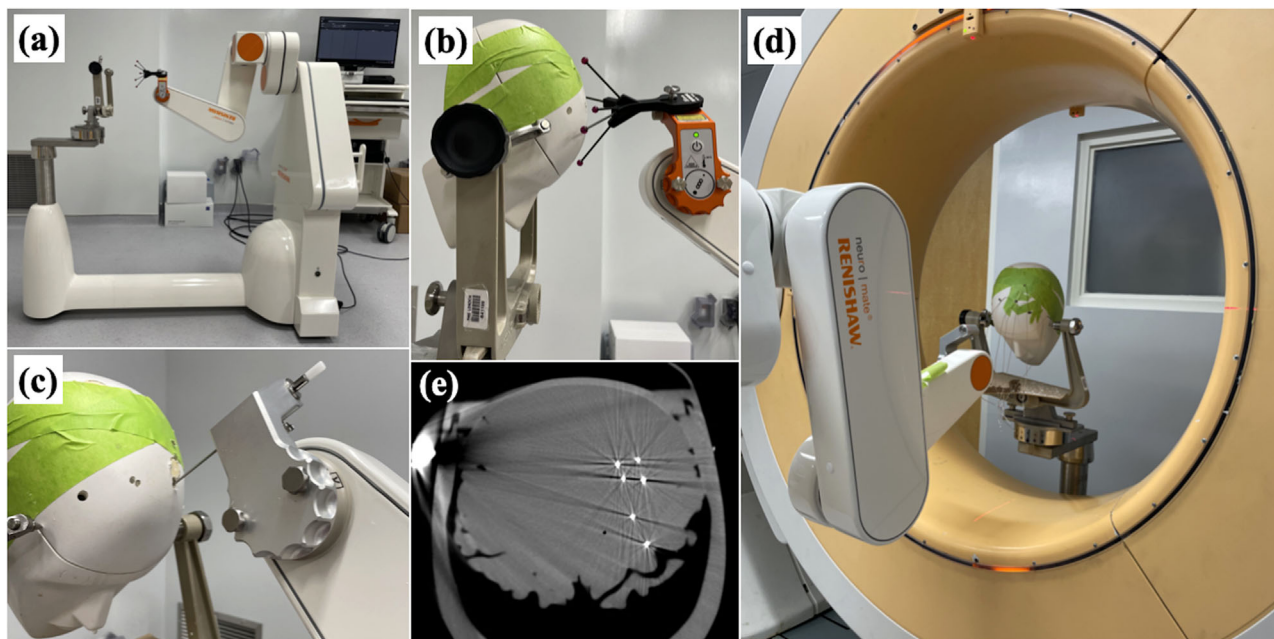

FIGURE 4 Robotic electrode implantation setup including (a) the Neuromate® robot with Mayfield® head frame and Neurolocate™ fiducial apparatus attached, and the workstation running the Neuroinspire™ electrode implantation planning system. (b) Phantom skull housing the brain phantom attached to the head frame with robot moved into Neurolocate™ registration position. (c) Cannula placement through drilled hole in skull at registered implant trajectory and depth. (d) CT imaging setup of postimplantation of electrodes and (e) the resulting CT image of the six implanted electrodes in the axial plane showing the four stimulating electrodes (top) and the two measurement electrodes (bottom)

placed through the cannula (Figure 4c) according to the optimization results, and the two recording electrodes were also implanted. CT imaging was acquired with a Medtronic O-Arm postimplantation (Figure 4d) and electrodes were successfully viewed in the resulting image (Figure 4e).

The planned voltage waveforms were applied to the four electrodes, with five active contacts on each electrode (Figure 5a), and the voltage over time was measured at the two recording electrodes. Measurements were also obtained from disconnected middle contacts on each active electrode (Figure 5b and c).
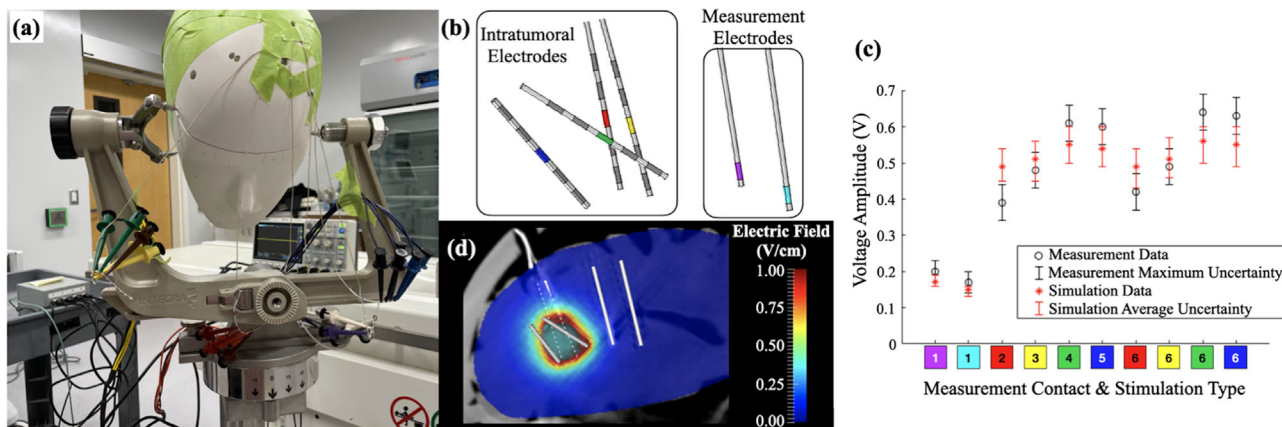
FIGURE 5 (a) Postimplantation phantom with four electrodes stimulated with four-channel waveform generator, connected to five contacts per electrode (20 total stimulating contacts), and two additional measurement electrodes. (b) Simulated geometry of electrode construct with measurement contacts highlighted in different colors. (c) Voltage measurement and simulation results, with colors corresponding to measurement contacts on electrode geometry, for various stimulation types (1: full 20 contact stimulation, 2–5: 19 contact stimulation with corresponding electrode contact replaced with measurement prong, and 6: 16 contact stimulation with all middle contacts replaced with measurement prongs). (d) Sagittal slice of postoperative treatment planning results with electric field superimposed on the CT and implanted electrodes projections (white) and tumor (cyan)

The frequency of all recorded continuous sinusoidal waveforms was 200 kHz ± 40 Hz. The postoperative CT was used to simulate the actual implant geometry (Figure 5b), with a calculated average Euclidian trajectory offset of 1.10 mm compared to the planned geometry. Simulation results of the voltage at measurement electrode contacts yielded electrical conductivity and dielectric of the phantom as 6.0 e-7 S/m and 5.0, respectively, and a conductivity of 5.0 e-4 S/m for the electrodes insulated section between electrode contacts.

Comparison between the measured voltage amplitudes and simulated voltages with maximum measurement and average simulation uncertainties are plotted in Figure 5c. Voltage amplitudes were recorded at the distal contacts on measurement electrodes for the planned 20 contact stimulation, and additional measurements were obtained for 19 contact stimulation and 16 contact stimulation, with corresponding active contacts (color highlighted contacts in Figure 5b) replaced with measurement probes (Figure 5c). Uncertainties in electrical properties and trajectories resulted in voltage simulation average uncertainties ranging from ±0.01 V to ±0.06 V. The uncertainty of electrical properties did not impact the tumor coverage within $p < 0.01$. The average 1.10 mm trajectory uncertainty of each electrode impacted the electric field tumor coverage by a maximum of 2.6%. The simultaneous measurement of voltage waveforms from the center contacts on the four stimulating electrodes allowed for validation of delivered phase shift between contacts within 5.8° average uncertainty, resulting in a maximum impact of 0.4% and average impact of 0.03% on electric field tumor coverage.

A postoperative plan using actual implant coordinates from the postoperative CT (Figure 4e) was performed to validate postoperative planning capability of the treatment planning system (Figure 5d). Postoperative planning found optimal parameters at actual implant locations as 2.20 V with phase shifts of 0°, 39.6°, 142.0°, 220.9° resulting in 95.4% tumor coverage with four active contacts on two electrodes, and five active contacts on the remaining two electrodes.

4 | DISCUSSION

In this study a custom IMT planning system was developed to map electric field distributions for human and preclinical models. 3D Slicer provided a suitable platform to create a custom coded Slicelet for our customized planning modules. External software modules were integrated into the system as background processes, removing user interaction with MeshLab, COMSOL, or MATLAB. The treatment planning pipeline was semiautomated, with fully automated COMSOL patient-specific model builds and MATLAB optimization code. Time-saving processes were also implemented into the MATLAB optimization, including the superposition of electric fields for objective calculation, custom mesh and interpolation matrix sizes, and rounding of parameters to 0.1 mm for location, 0.01 radians for phase shift, and 0.01 V for voltage amplitude. These updates resulted in an 8.3× speed improvement for location-based optimizations, and a 208× speed improvement for phase shift and voltage amplitude optimizations.

Different electrode types were utilized in the system including multi-contact human scale cylindrical

electrodes defined by insertion and tip coordinates, options for custom electrode arrays, and preclinical multi-electrode wire constructs. Electric field treatment parameters, including electrode locations, phase shifts and voltage amplitude were planned within the optimization module to maximize electric field coverage to the tumor over time. Conformity index optimization allowed for electric fields to be shaped in 3D to cover the tumor volume, while minimizing the field outside of the tumor. The optimized electric fields are visualized on interactive MRI slices, and the optimal geometry is visualized as a 3D model of the brain, tumor, and electrodes. The numerical results are displayed as parameter tables and the EVH graph to analyze the tumor volume and organ at risk coverage.

IMT is still in the early stages of development, and in order to move toward clinical trials, a treatment planning system is needed to determine the number of electrodes and their programming to accommodate tumors of different shape and size, located in any area of the brain. Different tumor types can also be considered, with electrical properties customizable for patient-specific brain and tumor characteristics. With initial electrode locations planned in the electrode implantation module, the treatment provider can ensure the electrode trajectories avoid any sensitive structures. Postoperative planning provides two essential capabilities, namely, the adjustment of parameters after electrode insertion, to account for the actual implantation coordinates, and the adjustment of treatment parameters over time as the tumor volume changes shape and size throughout treatment. Electrode encapsulation layer, brain shift, edema, and scarring over time can also be accounted for with postoperative stimulation reoptimization. The low-voltage nature of IMT (akin to DBS, which is regulated to ensure minimal tissue heating[65]) and active electrode contact placement within tumor tissue present minimal risk to nearby normal tissues. The surface charge density limit of 30 μC/cm^2 is considered to ensure electric fields are safely deliverable.[66] Organs at risk, such as the brainstem, were still considered in the IMT planning system, as electrode trajectories should not pass through these volumes. The optimization of electric field coverage considering the avoidance of sensitive structures and organs at risk was presented in previous work.[7]

The treatment planning system was validated by planning and robotically implanting four stimulating electrodes and two measurement electrodes in a brain phantom. The preoperative electrode configuration was implanted into the brain phantom and planned waveforms were applied to five contacts per electrode. Voltage measurements at the active contacts and recording electrodes demonstrated the capability to validate the voltage drop and electrical properties of the model postimplantation. When stimulations to middle contacts were replaced with measurement probes (Figure 5), measured voltages showed larger offsets from sim-

ulations compared to separate measurement probes placed ~1 cm from the closest active electrode, likely due to capacitive cross talk between recording and active wires within the same electrode. The accuracy of tip coordinate separation between electrode pairs was observed as 1.10 $\pm$ 0.60 mm.

Postoperative planning was validated using the actual implant coordinates localized with postimplant CT imaging. Measurements of the voltage surrounding the treated brain phantom found all but one voltage measurement was equal to simulations within the uncertainty. The bending of the electrodes is attributed to this offset between predicted and actual voltages. While the uncertainty in the simulation electrical property parameters affects the predicted voltage measurement, the overall electric field tumor coverage remains unaffected by these uncertainties. Trajectory uncertainties showed impact on both the voltage and electric field tumor coverage. The validation of delivered phase shift to within 1.6% provides insight on future treatment planning system updates to phase shift specificity.

Surgical electrode implantation of IMT electrodes will need to consider surgical and hardware complications associated with DBS and SEEG electrode implantation. Such risks remain low but include hemorrhage, infection, stroke, implant misplacement and migration, and component failure.[67,68] The success and tolerability of DBS long-term implantation support the potential of IMT to improve patient quality of life compared to external electric field devices, other ablation techniques, radiation, and chemotherapy. Limitations of the current planning pipeline include no differentiation between necrotic core and enhancing tumor segmentation, and long computation times (~4–8 h depending on the number of electrodes) required for location-based optimizations. The incorporation of necrotic core, white matter, gray matter, and cerebrospinal fluid (CSF) can be achieved in the future by additional segmentations and electrical parameter specification and could be implemented based on semiautomatic methods using specific MRI pulse sequences[69–71] and patient-specific electrical conductivity and permittivity maps.[72] Theoretically, since the active electrode contacts are within or directly adjacent the local tumor volume, the surrounding brain tissue inhomogeneities (white matter, gray matter, CSF) should not impact the results of the optimization, as has been supported by external field delivery studies.[5,73] The long computation times associated with location-based optimizations can be addressed in the future by utilizing parallel computing. Other future work will involve addressing the accuracy of the electric fields considering uncertainties from imaging, electrode localization, and finite element discretization and investigating custom electrode arrays for surgical resection cavities. Insights on the mechanisms of action will shape future updates to the planning system, including the importance and inclusion of electric field anisotropy

optimization. Concurrent in vitro and in vivo validations will lay a framework for a future single center safety trial.

The pipeline steps for planning an IMT treatment have been integrated into a single platform that consists of tissue segmentation, volume smoothing and simplification, electrode trajectory planning, electric field optimization, and results visualization. The amalgamation of planning steps in our custom semi-automated treatment planning system has improved the time to generate a treatment plan and the accessibility to the novice user. With the results of this study, the IMT optimization algorithm has been expanded to incorporate patient-specific scenarios, establishing a platform for future use in early-stage clinical investigations.

5 | CONCLUSION

The custom IMT treatment planning system and underlying optimization methods developed in this study provide an essential platform for future early clinical studies. The system provides a variety of planning options including preoperative and postoperative, surgical resection cavity models, and preclinical models, in addition to considerations of nearby organs at risk, tissue electrical properties, and prescription electric fields. The versatility of the system to patient-specific tumor shape and size, location, and tumor type will be evaluated in a future user study on large-scale patient data set planning. Overall, we have semiautomated and coalesced all IMT planning pipeline steps into a single user interface and validated the pipeline on a phantom model. This novel IMT treatment planning system will allow for future developments of IMT, progressing this technology toward clinical trials.

CONFLICT OF INTEREST
M.O.H. and S.S. are inventors on the following patent that is assigned to "London Health Sciences Centre Research Inc." (the applicant): CA2985847 entitled "Intratumoral Modulation Therapy." E.W., M.O.H., T.P., and S.S. are inventors on the following patent application that is assigned to "London Health Sciences Centre Research Inc." (the applicant): WO2021142549 entitled "Planning and delivery of dynamically oriented electric field for biomedical applications." The authors have no other competing interests.

REFERENCES

1. Stupp R, Wong ET, Kanner AA, et al. NovoTTF-100A versus physician's choice chemotherapy in recurrent glioblastoma: a randomised phase III trial of a novel treatment modality. *Eur J Cancer*. 2012;48(14):2192-2202. https://doi.org/10.1016/j.ejca.2012.04.011

2. Stupp R, Taillibert S, Kanner A, et al. Effect of tumor-treating fields plus maintenance temozolomide vs maintenance temozolomide alone on survival in patients with glioblastoma. *JAMA*. 2017;318(23):2306. https://doi.org/10.1001/jama.2017.18718

3. Hottinger AF, Pacheco P, Stupp R. Tumor treating fields: a novel treatment modality and its use in brain tumors. *Neuro Oncol*. 2016;18(10):1338-1349. https://doi.org/10.1093/neuonc/now182

4. Swanson KD, Lok E, Wong ET. An overview of alternating electric fields therapy (NovoTTF therapy) for the treatment of malignant glioma. *Curr Neurol Neurosci Rep*. 2016;16(1):8. https://doi.org/10.1007/s11910-015-0606-5

5. Wenger C, Miranda PC, Salvador R, et al. A review on tumor-treating fields (TTFields): clinical implications inferred from computational modeling. *IEEE Rev Biomed Eng*. 2018;11:195-207. https://doi.org/10.1109/RBME.2017.2765282

6. Shah PP, White T, Khalafallah AM, Romo CG, Price C, Mukherjee D. A systematic review of tumor treating fields therapy for high-grade gliomas. *J Neurooncol*. 2020;148(3):433-443. https://doi.org/10.1007/s11060-020-03563-z

7. Iredale E, Deweyert A, Hoover DA, et al. Optimization of multi-electrode implant configurations and programming for the delivery of non-ablative electric fields in intratumoral modulation therapy. *Med Phys*. 2020;47(11):5441-5454. https://doi.org/10.1002/mp.14496

8. Deweyert A, Iredale E, Xu H, Wong E, Schmid S, Hebb MO. Diffuse intrinsic pontine glioma cells are vulnerable to low intensity electric fields delivered by intratumoral modulation therapy. *J Neurooncol*. 2019;143(1):49-56. https://doi.org/10.1007/s11060-019-03145-8

9. Di Sebastiano AR, Deweyert A, Benoit S, et al. Preclinical outcomes of intratumoral modulation therapy for glioblastoma. *Sci Rep*. 2018;8(1):7301. https://doi.org/10.1038/s41598-018-25639-7

10. Xu H, Bihari F, Whitehead S, Wong E, Schmid S, Hebb MO. In vitro validation of intratumoral modulation therapy for glioblastoma. *Anticancer Res*. 2016;36:71-80.

11. Rominiyi O, Vanderlinden A, Clenton SJ, Bridgewater C, Al-Tamimi Y, Collis SJ. Tumour treating fields therapy for glioblastoma: current advances and future directions. *Br J Cancer*. 2021;124(4):697-709. https://doi.org/10.1038/s41416-020-01136-5

12. Tuszynski J, Wenger C, Friesen D, Preto J. An overview of subcellular mechanisms involved in the action of TTFields. *Int J Environ Res Public Health*. 2016;13(11):1128. https://doi.org/10.3390/ijerph13111128

13. Carrieri FA, Smack C, Siddiqui I, Kleinberg LR, Tran PT. Tumor treating fields: at the crossroads between physics and biology for cancer treatment. *Front Oncol*. 2020;10. https://doi.org/10.3389/fonc.2020.575992

14. Li X, Yang F, Rubinsky B. A correlation between electric fields that target the cell membrane potential and dividing HeLa cancer cell growth inhibition. *IEEE Trans Biomed Eng*. 2021;68(6):1951-1956. https://doi.org/10.1109/TBME.2020.3042650

15. Li X, Yang F, Rubinsky B. A theoretical study on the biophysical mechanisms by which tumor treating fields affect tumor cells during mitosis. *IEEE Trans Biomed Eng*. 2020;67(9):2594-2602. https://doi.org/10.1109/TBME.2020.2965883

16. Kirson ED, Gurvich Z, Schneiderman R, et al. Disruption of cancer cell replication by alternating electric fields. *Cancer Res*. 2004;64(9):3288-3295. https://doi.org/10.1158/0008-5472.CAN-04-0083

17. Kirson ED, Dbalý V, Tovaryš F, et al. Alternating electric fields arrest cell proliferation in animal tumor models and human brain tumors. *Proc Natl Acad Sci*. 2007;104(24):10152-10157. https://doi.org/10.1073/pnas.0702916104

18. Giladi M, Schneiderman RS, Voloshin T, et al. Mitotic spindle disruption by alternating electric fields leads to improper chromosome segregation and mitotic catastrophe in cancer cells. *Sci Rep*. 2016;5(1):18046. https://doi.org/10.1038/srep18046

19. Chang E, Patel CB, Pohling C, et al. Tumor treating fields increases membrane permeability in glioblastoma cells. *Cell Death Discov*. 2018;4(1):113. https://doi.org/10.1038/s41420-018-0130-x

20. Connelly J, Hormigo A, Mohilie N, Hu J, Chaudhry A, Blondin N. Planning TTFields treatment using the NovoTAL system-clinical case series beyond the use of MRI contrast enhancement. *BMC Cancer*. 2016;16(1):842. https://doi.org/10.1186/s12885-016-2890-0

21. Chaudhry A, Benson L, Varshaver M, et al. NovoTTF™-100A System (Tumor Treating Fields) transducer array layout planning for glioblastoma: a NovoTAL™ system user study. *World J Surg Oncol*. 2015;13(1):316. https://doi.org/10.1186/s12957-015-0722-3

22. Benson L. Tumor treating fields technology: alternating electric field therapy for the treatment of solid tumors. *Semin Oncol Nurs*. 2018;34(2):137-150. https://doi.org/10.1016/j.soncn.2018.03.005

23. Wenger C, Salvador R, Basser PJ, Miranda PC. Improving tumor treating fields treatment efficacy in patients with glioblastoma using personalized array layouts. *Int J Radiat Oncol*. 2016;94(5):1137-1143. https://doi.org/10.1016/j.ijrobp.2015.11.042

24. Korshoej AR, Sørensen JCH, von Oettingen G, Poulsen FR, Thielscher A. Optimization of tumor treating fields using singular value decomposition and minimization of field anisotropy. *Phys Med Biol*. 2019;64(4):04NT03. https://doi.org/10.1088/1361-6560/aafe54

25. Adair DSP, Gomes KS, Kiss ZHT, Gobbi DG, Starreveld YP. Tactics: an open-source platform for planning, simulating and validating stereotactic surgery. *Comput Assist Surg*. 2020;25(1):1-14. https://doi.org/10.1080/24699322.2020.1760354

26. Bériault S, Al SubaieF, Collins DL, Sadikot AF, Pike GB. A multi-modal approach to computer-assisted deep brain stimulation trajectory planning. *Int J Comput Assist Radiol Surg*. 2012;7(5):687-704. https://doi.org/10.1007/s11548-012-0768-4

27. Liu Y, Konrad PE, Neimat JS, et al. Multisurgeon, multisite validation of a trajectory planning algorithm for deep brain stimulation procedures. *IEEE Trans Biomed Eng*. 2014;61(9):2479-2487. https://doi.org/10.1109/TBME.2014.2322776

28. Essert C, Fernandez-Vidal S, Capobianco A, et al. Statistical study of parameters for deep brain stimulation automatic preoperative planning of electrodes trajectories. *Int J Comput Assist Radiol Surg*. 2015;10(12):1973-1983. https://doi.org/10.1007/s11548-015-1263-5

29. Essert C, Haegelen C, Lalys F, Abadie A, Jannin P. Automatic computation of electrode trajectories for deep brain stimulation: a hybrid symbolic and numerical approach. *Int J Comput Assist Radiol Surg*. 2012;7(4):517-532. https://doi.org/10.1007/s11548-011-0651-8

30. Krauss JK, Lipsman N, Aziz T, et al. Technology of deep brain stimulation: current status and future directions. *Nat Rev Neurol*. 2021;17(2):75-87. https://doi.org/10.1038/s41582-020-00426-z

31. Garcia PA, Kos B, Rossmeisl JH, Pavliha D, Miklavčič D, Davalos RV. Predictive therapeutic planning for irreversible electroporation treatment of spontaneous malignant glioma. *Med Phys*. 2017;44(9):4968-4980. https://doi.org/10.1002/mp.12401

32. Stillström D, Sandu R-M, Freedman J. Accuracy of electrode placement in IRE treatment with navigated guidance. *Cardiovasc Intervent Radiol*. 2021;44(6):968-975. https://doi.org/10.1007/s00270-020-02762-5

33. Ding L, Moser M, Luo Y, Zhang W, Zhang B. Treatment planning optimization in irreversible electroporation for complete ablation of variously sized cervical tumors: a numerical study. *J Biomech Eng*. 2021;143(1). https://doi.org/10.1115/1.4047551

34. Edd JF, Davalos RV. Mathematical modeling of irreversible electroporation for treatment planning. *Technol Cancer Res Treat*. 2007;6(4):275-286. https://doi.org/10.1177/153303460700600403

35. Gong L, Yao C, Dong S, Zhao Y. The optimization of the treatment planning for achieving complete ablation of tumor during irreversible electroporation by genetic algorithm. In: *2017 IEEE 21st International Conference on Pulsed Power (PPC)*. IEEE; 2017:1-6. https://doi.org/10.1109/PPC.2017.8291223

36. Vakharia VN, Sparks R, Miserocchi A, et al. Computer-assisted planning for stereoelectroencephalography (SEEG). *Neurotherapeutics*. 2019;16(4):1183-1197. https://doi.org/10.1007/s13311-019-00774-9

37. Nowell M, Sparks R, Zombori G, et al. Comparison of computer-assisted planning and manual planning for depth electrode implantations in epilepsy. *J Neurosurg*. 2016;124(6):1820-1828. https://doi.org/10.3171/2015.6.JNS15487

38. González-Martínez J, Bulacio J, Thompson S, et al. Technique, results, and complications related to robot-assisted stereoelectroencephalography. *Neurosurgery*. 2016;78(2):169-180. https://doi.org/10.1227/NEU.0000000000001034

39. Narayanasamy G, Saenz DL, Defoor D, Papanikolaou N, Stathakis S. Dosimetric validation of Monaco treatment planning system on an Elekta VersaHD linear accelerator. *J Appl Clin Med Phys*. 2017;18(6):123-129. https://doi.org/10.1002/acm2.12188

40. Peters S, Schiefer H, Plasswilm L. A treatment planning study comparing Elekta VMAT and fixed field IMRT using the varian treatment planning system eclipse. *Radiat Oncol*. 2014;9(1):153. https://doi.org/10.1186/1748-717X-9-153

41. Ding C, Saw CB, Timmerman RD. Cyberknife stereotactic radiosurgery and radiation therapy treatment planning system. *Med Dosim*. 2018;43(2):129-140. https://doi.org/10.1016/j.meddos.2018.02.006

42. Bodensteiner D. RayStation: external beam treatment planning system. *Med Dosim*. 2018;43(2):168-176. https://doi.org/10.1016/j.meddos.2018.02.013

43. Mzenda B, Mugabe KV, Sims R, Godwin G, Loria D. Modeling and dosimetric performance evaluation of the RayStation treatment planning system. *J Appl Clin Med Phys*. 2014;15(5):29-46. https://doi.org/10.1120/jacmp.v15i5.4787

44. Xia P, Murray E. 3D treatment planning system—pinnacle system. *Med Dosim*. 2018;43(2):118-128. https://doi.org/10.1016/j.meddos.2018.02.004

45. Jameson MG, Ohanessian L, Batumalai V, Patel V, Holloway LC. Comparison of Oncentra ® Brachy IPSA and graphical optimisation techniques: a case study of HDR brachytherapy head and neck and prostate plans. *J Med Radiat Sci*. 2015;62(2):168-174. https://doi.org/10.1002/jmrs.107

46. Shwetha B, Ravikumar M, Supe SS, Sathiyan S, Lokesh V, Keshava SL. Dosimetric evaluation of two treatment planning systems for high dose rate brachytherapy applications. *Med Dosim*. 2012;37(1):71-75. https://doi.org/10.1016/j.meddos.2010.12.015

47. 3D Slicer. 3D Slicer image computing platform. https://www.slicer.org

48. Fedorov A, Beichel R, Kalpathy-Cramer J, et al. 3D Slicer as an image computing platform for the quantitative imaging network. *Magn Reson Imaging*. 2012;30(9):1323-1341. https://doi.org/10.1016/j.mri.2012.05.001

49. Renishaw. neuromate® robotic system for stereotactic neurosurgery. https://www.renishaw.com/en/neuromate-robotic-system-for-stereotactic-neurosurgery–10712

50. 3D Slicer. Slicelets. https://www.slicer.org/wiki/Documentation/Nightly/Developers/Slicelets

51. 3D Slicer. Models Module. https://www.slicer.org/wiki/Documentation/4.3/Modules/Volumes

52. 3D Slicer. Volumes Module. https://www.slicer.org/wiki/Documentation/4.3/Modules/Volumes

53. Wenger C, Salvador R, Basser PJ, Miranda PC. The electric field distribution in the brain during TTFields therapy and its dependence on tissue dielectric properties and anatomy: a computational study. *Phys Med Biol*. 2015;60(18):7339-7357. https://doi.org/10.1088/0031-9155/60/18/7339

54. Korshoej AR, Saturnino GB, Rasmussen LK, von Oettingen G, Sørensen JCH, Thielscher A. Enhancing predicted efficacy of tumor treating fields therapy of glioblastoma using targeted surgical craniectomy: a computer modeling study. *PLoS One*. 2016;11(10):e0164051. https://doi.org/10.1371/journal.pone.0164051

55. Miranda PC, Mekonnen A, Salvador R, Basser PJ. Predicting the electric field distribution in the brain for the treatment of glioblastoma. *Phys Med Biol*. 2014;59(15):4137-4147. https://doi.org/10.1088/0031-9155/59/15/4137

56. Korshoej AR, Hansen FL, Thielscher A, von Oettingen GB, Sørensen JCH. Impact of tumor position, conductivity distribution and tissue homogeneity on the distribution of tumor treating fields in a human brain: a computer modeling study. *PLoS One*. 2017;12(6):e0179214. https://doi.org/10.1371/journal.pone.0179214

57. Gabriel C, Peyman A, Grant EH. Electrical conductivity of tissue at frequencies below 1 MHz. *Phys Med Biol*. 2009;54(16):4863-4878. https://doi.org/10.1088/0031-9155/54/16/002

58. Latikka J, Kuurne T, Eskola H. Conductivity of living intracranial tissues. *Phys Med Biol*. 2001;46(6):1611-1616. https://doi.org/10.1088/0031-9155/46/6/302

59. Stoy RD, Foster KR, Schwan HP. Dielectric properties of mammalian tissues from 0.1 to 100 MHz; a summary of recent data. *Phys Med Biol*. 1982;27(4):501-513. https://doi.org/10.1088/0031-9155/27/4/002

60. Latikka J, Eskola H. The resistivity of human brain tumours in vivo. *Ann Biomed Eng*. 2019;47(3):706-713. https://doi.org/10.1007/s10439-018-02189-7

61. 3D Slicer. Sample data. https://www.slicer.org/wiki/SampleData

62. Synaptive Medical. BrightMatter™ Simulate: remarkably lifelike brain tissue models. https://www.synaptivemedical.com/products/simulate/

63. Butson CR, McIntyre CC. Role of electrode design on the volume of tissue activated during deep brain stimulation. *J Neural Eng*. 2006;3(1):1-8. https://doi.org/10.1088/1741-2560/3/1/001

64. Renishaw neuroinspire™ neurosurgical planning software. https://www.renishaw.com/en/neuroinspire-neurosurgical-planning-software-8244

65. Elwassif MM, Datta A, Rahman A, Bikson M. Temperature control at DBS electrodes using a heat sink: experimentally validated FEM model of DBS lead architecture. *J Neural Eng*. 2012;9(4):046009. https://doi.org/10.1088/1741-2560/9/4/046009

66. Cogan SF, Ludwig KA, Welle CG, Takmakov P. Tissue damage thresholds during therapeutic electrical stimulation. *J Neural Eng*. 2016;13(2):021001. https://doi.org/10.1088/1741-2560/13/2/021001

67. Fenoy AJ, Simpson RK. Risks of common complications in deep brain stimulation surgery: management and avoidance. *J Neurosurg*. 2014;120(1):132-139. https://doi.org/10.3171/2013.10.JNS131225

68. Mullin JP, Shriver M, Alomar S, et al. Is SEEG safe? A systematic review and meta-analysis of stereo-electroencephalography-related complications. *Epilepsia*. 2016;57(3):386-401. https://doi.org/10.1111/epi.13298

69. Singh MK, Singh KK. A review of publicly available automatic brain segmentation methodologies, machine learning models, recent advancements, and their comparison. *Ann Neurosci*. 2021;28(1-2):82-93. https://doi.org/10.1177/0972753121990175

70. Wang Y, Wang Y, Zhang Z, et al. Segmentation of gray matter, white matter, and CSF with fluid and white matter suppression using MP2RAGE. *J Magn Reson Imaging*. 2018;48(6):1540-1550. https://doi.org/10.1002/jmri.26014

71. Dora L, Agrawal S, Panda R, Abraham A. State-of-the-art methods for brain tissue segmentation: a review. *IEEE Rev Biomed Eng*. 2017;10:235-249. https://doi.org/10.1109/RBME.2017.2715350

72. Michel E, Hernandez D, Lee SY. Electrical conductivity and permittivity maps of brain tissues derived from water content based on T_1-weighted acquisition. *Magn Reson Med*. 2017;77(3):1094-1103. https://doi.org/10.1002/mrm.26193

73. Wenger C, Bomzon Z, Salvador R, Basser PJ, Miranda PC. Simplified realistic human head model for simulating Tumor Treating Fields (TTFields). In *2016 38th Annual International Conference of the IEEE Engineering in Medicine and Biology Society (EMBC)*. Vol 2016-October. IEEE; 2016:5664-5667. https://doi.org/10.1109/EMBC.2016.7592012

SUPPORTING INFORMATION

Additional supporting information can be found online in the Supporting Information section at the end of this article.